EUROPEAN ORGANIZATION FOR NUCLEAR RESEARCH

CERN-EP/83-85
27 June 1983

PHOTOPRODUCTION OF $\pi^+\pi^-\pi^0$ ON HYDROGEN WITH LINEARLY POLARIZED PHOTONS OF ENERGY 20-70 GeV

Bonn[1]-CERN[2]-Glasgow[3]-Lancaster[4]-Manchester[5]-Paris VI[6]-Rutherford[7]-Sheffield[8] Collaboration

M. Atkinson[7], T.J. Axon[5], D. Barberis[5], T.J. Brodbeck[4], G.R. Brookes[8], J.J. Bunn[8], P.J. Bussey[3], A.B. Clegg[4], J.B. Dainton[3], M. Davenport[7], B. Dickinson[5], B. Diekmann[1], A. Donnachie[5], R.J. Ellison[5], P. Flower[7], P.J. Flynn[4], W. Galbraith[8], K. Heinloth[1], R.C.W. Henderson[4], R.E. Hughes-Jones[5], J.S. Hutton[7], M. Ibbotson[5], H.P. Jakob[1], M. Jung[1], M.A.R. Kemp[7], B.R. Kumar[7], J. Laberrigue[6], G.D. Lafferty[5], J.B. Lane[5], J.C. Lassalle[2], J.M. Lévy[6], V. Liebenau[1], R.H. McClatchey[8], D. Mercer[5], J.A.G. Morris[7], J.V. Morris[7], D. Newton[4], C. Paterson[3], G.N. Patrick[2], E. Paul[1], C. Raine[3], M. Reidenbach[1], H. Rotscheidt[1], A. Schlösser[1], P.H. Sharp[7], I.O. Skillicorn[3], K.M. Smith[3], K.M. Storr[2], R.J. Thompson[5], Ch. de la Vaissière[6], A.P. Waite[5] and T.P. Yiou[6]

(The Omega Photon Collaboration)

(Submitted to Nuclear Physics B)

ABSTRACT

Results on photoproduction of $\pi^+\pi^-\pi^0$ in the photon energy range 20-70 GeV are presented. For the ω meson, the production cross-section is found to be 1010 ± ± 15 (statistical) ± 290 (systematic) nb and is constant over the incident photon energy range. Spin-density matrix elements are evaluated for ω meson production. The ϕ meson is observed with a total photoproduction cross-section [corrected for branching ratio (B) to $\pi^+\pi^-\pi^0$] of 610 ± 35 ± 170 nb. A third resonance, at 1.67 GeV, is seen in the mass spectrum and its interpretation is discussed. The production of a broad $\pi^+\pi^-\pi^0$ continuum, mainly via $\rho\pi$, and peaking at 1.2 GeV, contributes with a cross-section of about 2.5 μb. The spin-parity content is analysed by the moments of the $\pi^+\pi^-\pi^0$ decay angular distribution in the helicity frame and by maximum likelihood fits to the $\pi^+\pi^-\pi^0$ Dalitz plot. It is found that production of $J^P = 1^-$ states accounts for less than half of the total mass spectrum above 900 MeV. There is a broad enhancement in the 1^+ wave around 1.15 GeV indicating photoproduction of the H(1190) meson.

1. INTRODUCTION

Data are presented on the reaction

$$\gamma p \to \pi^+\pi^-\pi^0 p \tag{1}$$

from a study of the photoproduction of hadrons by linearly polarized tagged photons of energy 20 to 70 GeV. The experiment (WA57) was performed using the Omega spectrometer at the CERN SPS.

In this paper the following subprocesses of reaction (1), involving vector-meson production are considered:

$$\gamma p \to \omega p \to \pi^+\pi^-\pi^0 p \tag{2}$$

$$\gamma p \to \phi p \to \pi^+\pi^-\pi^0 p \tag{3}$$

and

$$\gamma p \to \text{"}\omega'(1670)\text{"} p \to \pi^+\pi^-\pi^0 p \tag{4}$$

where "$\omega'(1670)$" refers to the peak in the mass spectrum at 1.67 GeV which has already been reported [1]. In addition to these three resonances there is an indication of production of the H(1190) meson, and there is also production of a continuum of 3π states.

In the case of ω photoproduction it is known that unnatural spin-parity exchange is an important contribution at photon energies below 10 GeV [2], while at higher energies it is consistent with a purely natural parity exchange process [3-5]. In the present experiment, the linear polarization of the photon beam is used to study the naturality of the exchange process in high-energy ω photoproduction via reaction (2).

High-energy photoproduction of ϕ mesons has previously been studied in the K^+K^- decay mode [6,7]; in this experiment the $\pi^+\pi^-\pi^0$ decay mode, which is seen in the mass spectrum with a large background from the $\pi^+\pi^-\pi^0$ continuum, is studied in reaction (3).

Details of the production of a third resonance via reaction (4) have already been reported [1]. In this paper further details are discussed, and for convenience the resonance is labelled as "$\omega'(1670)$".

The production of continuum 3π states above the ω mass is found to contribute to reaction (1) with a cross-section which is large enough to allow a detailed study of these states in this experiment. In particular the spin-parity content has been investigated via the moments of the decay angular distributions and by an analysis of the Dalitz-plot distributions as functions of 3π mass.

2. EXPERIMENTAL SET-UP AND DATA

An 80 GeV electron beam at the CERN SPS was used to generate a partially plane polarized beam of photons by means of coherent bremsstrahlung in a silicon crystal [8,9]. The photon momenta were tagged in the range 20-70 GeV.

The distributions of incident photon energy and polarization intensity (calculated as described in ref. 9) are shown in fig. 1. These were monitored by a subsidiary unbiased trigger, which merely required a signal from an end-cap scintillation counter immediately following the hydrogen target. Approximately half of the data were taken with the plane of photon polarization at $+45^\circ$ to the median plane and the other half at -45° (these are conventionally labelled as negative and positive values of polarization, P_γ, in fig. 1c). The mean polarization, averaged over the photon energy spectrum, was 0.3.

The photons entered the Omega spectrometer which was equipped with a 60 cm long liquid-hydrogen target, multiwire proportional chambers and, downstream of the magnet, drift chambers (DC1 and DC2), a threshold Čerenkov counter and a photon detector. The layout is shown in fig. 2 and has been described elsewhere [10]. The photon detector comprised an active converter (sampler), made up of 42 slabs of lead-glass, each of three radiation lengths in depth, followed by a shower position detector hodoscope (Penelope) of 792 scintillation counters, and finally an array of 343 lead-glass blocks (Olga) each of area 140×140 mm^2 and depth

500 mm ($\sim$ 20 radiation lengths). The calorimeter subtended a solid angle of 0.07 sr about the forward direction and measured the photon direction to an accuracy of ±0.2 mrad.

Events for reaction (1) came from a trigger which required between two and five forward charged particles plus a signal from the lead-glass array indicating the detection of at least one γ-ray of energy above 2 GeV. Electromagnetic background was reduced by a system of veto counters in the median plane consisting of the median row blocks of the lead-glass array plus additional electron veto counters (EVAs) (see fig. 2). Pattern recognition and geometrical reconstruction of the events were performed by the program TRIDENT [11]. A second program performed the auxiliary tasks of reconstructing the momentum and polarization of the incident photons, decoding the Čerenkov information for particle identification, and reconstructing γ-rays and π^0 mesons. Event selection for channel (1) required a well-measured primary photon, two or three charged particles consistent with $\pi^+\pi^-$ or $\pi^+\pi^-$p, respectively, to be reconstructed to a single vertex in the hydrogen target, and two γ-rays to form a π^0.

From the interaction of 5.6×10^{10} photons with 2.54×10^{24} protons/cm^2 of the hydrogen target, a total of $\sim$ 40,000 candidates for reaction (1) was obtained. One-constraint fits were performed to π^0's for $\gamma\gamma$ pairs in the mass range $120 < < M_{\gamma\gamma} < 150$ MeV. Figure 3 shows the distribution of missing mass squared to $\pi^+\pi^-\pi^0$ for all candidate events; final selection of channel (1) required missing mass squared less than 5 GeV^2 leaving a final sample of 14,236 events, about 15% of which are background from processes other than reaction (1). The mass spectrum of $\gamma\gamma$ for events selected as described above, but before the π^0 fit selection, is shown in fig. 4; the background in channel (1) from non-π^0 $\gamma\gamma$ pairs is about 5%.

The final $\pi^+\pi^-\pi^0$ mass spectrum is shown in fig. 5 and indicates a strong ω signal and smaller signals from ϕ and "$\omega'(1670)$" over a substantial continuum background.

3. ACCEPTANCE

In order to calculate the acceptance of the events, reactions (2), (3), (4), and a $\pi^+\pi^-\pi^0$ mass continuum were simulated by a Monte Carlo program [12]. The photon bremsstrahlung spectrum was generated with the shape as determined by the monitor trigger discussed above; the production cross-sections were taken to be independent of photon energy, and the differential cross-sections, $d\sigma/dt$, were taken as exponential with slopes of 7 GeV^{-2} for ω production, 5 GeV^{-2} for ϕ production, and 5 GeV^{-2} for "$\omega'(1670)$" and the continuum. The angular distribution, $W(\cos\theta, \phi, \Phi)$, of the normal to the $\pi^+\pi^-\pi^0$ decay plane in the s-channel helicity system*) (fig. 6) was chosen to be proportional to $\sin^2\theta$ for the ω and otherwise to be flat. The generated events were passed through an acceptance program [14], which simulated the experimental conditions including the multiplicity requirements of the trigger, the geometrical cuts imposed by the apparatus, and the inefficiencies of the chambers. This program also included a detailed simulation of showering in the photon calorimeter, Olga. A bin-by-bin division of the spectra for accepted events by those for generated events then yielded the acceptance as a function of beam momentum, $\pi^+\pi^-\pi^0$ mass, t, and the angles θ, ϕ, and Φ. The variation of acceptance in all the variables was small for the kinematic ranges studied and, in particular, the acceptance function, $A(k_\gamma, M_{3\pi}, t, \theta, \phi, \Phi)$, was nowhere equal to zero. The overall acceptance obtained for the model described is shown as a function of $\pi^+\pi^-\pi^0$ mass in fig. 5; above the ω mass region, an assumption for the distribution in $\cos\theta$ of $\sin^2\theta$ or $(1 + \cos^2\theta)$, rather than isotropy, would change the acceptance by only -10% and +5%, respectively, of the value indicated.

---

*) In the helicity frame, the z-axis is the direction of the 3π system in the overall γp c.m.s. The y-axis is the normal to the production plane given by the cross-product of the photon and 3π directions. The x-axis is given by $\hat{\underset{\sim}{x}} = \hat{\underset{\sim}{y}} \times \hat{\underset{\sim}{z}}$. The angle Φ between the electric vector of the photon, $\underset{\sim}{\varepsilon}_\gamma$, and the production plane in the c.m.s. is defined by $\sin\Phi = \underset{\sim}{y} \cdot \underset{\sim}{\varepsilon}$ and $\cos\Phi = \underset{\sim}{\varepsilon}_\gamma \cdot (\underset{\sim}{y} \times \underset{\sim}{k})$, where $\underset{\sim}{k}$ is the photon direction [13].

4. RESULTS

4.1 Photoproduction of ω mesons

In fig. 7 the $\pi^+\pi^-\pi^0$ mass spectrum in the ω peak region is shown and is compared with the corresponding distribution for simulated events, where smearing of the track momenta has been applied to account for the measurement errors. The ω peak is well reproduced by the Monte Carlo simulation, indicating a mass resolution of $\sigma \simeq 15$ MeV.

The total cross-section for ω photoproduction in the mass range $0.72 < M_{\pi^+\pi^-\pi^0} < 0.86$ GeV has been calculated from the number of observed events after subtraction of the background shown in fig. 7 (this background is required to obtain good agreement between the Monte Carlo simulation of the Omega shape and the data). Corrections for the following effects have been applied (a-e are from the simulation):

a) overall trigger acceptance;

b) geometrical aperture acceptance;

c) pattern recognition and reconstruction inefficiencies;

d) conversion of γ-rays from π^0 decay in the magnetic field;

e) misassignment of particle type owing to inefficiency of the Čerenkov counter;

f) reconstruction efficiency for beam photons;

g) interaction of secondary $\pi^\pm$ in the apparatus;

h) branching ratio of ω to $\pi^+\pi^-\pi^0$;

i) losses due to the cut on missing mass squared.

With these corrections, the cross-section, averaged over the beam energy range 20-70 GeV, is

$$\sigma(\gamma p \to \omega p) = 1010 \pm 15 \text{ (statistical)} \pm 290 \text{ (systematic) nb} ,$$

in agreement with previous determinations [3,4].

The cross-section, $\sigma(\gamma p \to \omega p)$, is shown as a function of beam energy E_γ in fig. 8, and is seen to be only weakly dependent on photon energy. Such behaviour would be expected in the case of a simple diffractive production mechanism. A fit to the data of the form:

$$\sigma = \sigma_0 E_\gamma^n$$

yields

$$n = -0.12 \pm 0.09 \ .$$

In fig. 9 is shown the $dN(\gamma p \to \omega p)/dt$ for three intervals of photon energy. These distributions were fitted to the forms

$$\frac{dN}{dt} = a \exp(bt) \quad \text{and} \quad \frac{dN}{dt} = a \exp(bt + ct^2) \ ,$$

in the range $0.02 < -t < 0.8$ GeV^2, and the resulting values of b and c are given in table 1. On an average over the whole photon-energy range (20-70 GeV), the values were, for the first fit: $b = -7.3 \pm 0.2$ GeV^{-2}, and, for the second fit: $b = -9.2 \pm 0.1$ GeV^{-2} and $c = 3.9 \pm 0.2$ GeV^{-4}. These slope parameters are consistent with results from ρ^0 photoproduction in the same energy range [3], thus confirming the dominantly diffractive nature of the ω production mechanism [15].

The decay angular distributions of the ω in the s-channel helicity system in terms of $\cos\theta$ and $\psi = \phi - \Phi$ (see fig. 6 and ref. 2) are shown in fig. 10. The corresponding (acceptance-corrected) spherical harmonic moments $\langle Y_\ell^m(\cos\theta,\psi)\rangle$, were studied as a function of $\pi^+\pi^-\pi^0$ mass for values of ℓ up to 6. Table 2 gives, normalized to $\langle Y_0^0\rangle$, the moments in the ω mass range for ℓ up to 2, with m up to 2, and higher moments for m = 0. All other moments were found to be consistent with zero.

The moments $\langle Y_2^0\rangle$ and $\langle \mathrm{Re}\ Y_2^2\rangle$ give substantial contributions in the ω mass range (there is in addition a small signal in $\langle \mathrm{Re}\ Y_2^1\rangle$), and show no variation with mass within the range 0.72-0.86 GeV. In fact these are expected to be the only two non-vanishing moments for s-channel helicity conserving (SCHC) P-wave states, since the decay angular distribution is then given by [see eqs. (6) and (7)]:

$$W(\cos\theta, \psi) = \frac{1}{\sqrt{4\pi}} Y_0^0 - \frac{1}{\sqrt{20\pi}} Y_2^0(\cos\theta) + 2P_\gamma \sqrt{\frac{3}{40\pi}} \text{Re}\, Y_2^2(\cos\theta, \psi) \ , \qquad (5)$$

where P_γ is the mean linear polarization of the photon beam. In the approximation that the $\pi^+\pi^-\pi^0$ production in the ω mass region is uniquely described by eq. (5), independent cross-section values for production of SCHC P-wave states can be obtained from $\langle Y_2^0 \rangle$ and $\langle Y_2^2 \rangle$. These are (with statistical errors only):

$$\sigma_{SCHC}(\gamma p \to \omega p) = - \sqrt{20\pi} \langle Y_2^0 \rangle = 0.830 \pm 50 \ \mu b$$

and

$$\sigma_{SCHC}(\gamma p \to \omega p) = \frac{1}{P_\gamma} \sqrt{\frac{40\pi}{3}} \langle \text{Re}\, Y_2^2 \rangle = 0.930 \pm 120 \ \mu b \ .$$

For a more detailed study of the ω production mechanism, the decay angular distribution is considered in terms of nine independent, measurable spin-density matrix elements [13], $\rho^\alpha_{mm'}$:

$$\begin{aligned} W(\cos\theta, \phi, \Phi) = \frac{3}{4\pi} \big[& \tfrac{1}{2}(1 - \rho^0_{00}) \\ & + (3\rho^0_{00} - 1) \cos^2\theta - \sqrt{2}\, \text{Re}\, \rho^0_{10} \sin 2\theta \cos\phi \\ & - \rho^0_{1-1} \sin^2\theta \cos 2\phi - P_\gamma \cos 2\Phi (\rho^1_{11} \sin^2\theta + \rho^1_{00} \cos^2\theta \\ & - \sqrt{2}\, \text{Re}\, \rho^1_{10} \sin 2\theta \cos\phi - \rho^1_{1-1} \sin^2\theta \cos 2\phi) \\ & - P_\gamma \sin 2\Phi \, (\sqrt{2}\, \text{Im}\, \rho^2_{10} \sin 2\theta \sin\phi \\ & + \text{Im}\, \rho^2_{1-1} \sin^2\theta \sin 2\phi) \big] \ . \end{aligned} \qquad (6)$$

The $\rho^\alpha_{mm'}$ have been evaluated in the helicity frame using the method of moments (the methods of least squares and maximum likelihood have also been used and give consistent results); the results are given in table 3 for the 3π mass range 0.72-0.84 GeV and E_γ range 20-70 GeV. No significant variation of the $\rho^\alpha_{mm'}$ was found across these ranges. If the ω production mechanism conserves s-channel helicity (i.e. the ω is transverse and linearly polarized like the photon) and proceeds by natural parity exchange, then

$$\rho^1_{1-1} = -\text{Im}\, \rho^2_{1-1} = \tfrac{1}{2} \qquad (7)$$

and all other ρ^{α}_{mm}, [in eq. (6)] would be zero. The results in table 3 are consistent with these predictions, allowing for the small background under the ω meson peak.

The contributions to the total cross-section from natural (N) and unnatural (U) parity exchange have been calculated using [2]:

$$\sigma^N - \sigma^U = (2\rho^1_{1-1} - \rho^1_{00})\sigma^{tot} \tag{8}$$

giving

$$\sigma^N = 920 \pm 70 \text{ nb}$$

$$\sigma^U = 90 \pm 70 \text{ nb} .$$

These values are consistent with the value of $\sigma^U \approx 0$ expected on the basis of previous ω photoproduction results at 9.3 GeV photon energy [2].

4.2 Photoproduction of φ mesons

Figure 11 shows the $\pi^+\pi^-\pi^0$ mass spectrum in the φ region. The φ meson is seen with a width corresponding to the experimental mass resolution, at this mass, of $\sigma \approx 20$ MeV. The cross-section was determined by a fit to a Gaussian distribution plus a polynomial background (shown as full curve in fig. 11) to be

$$\sigma(\gamma p \to \phi p)B(\phi \to \pi^+\pi^-\pi^0) = 90 \pm 5 \text{ (stat.)} \pm 25 \text{ (syst.) nb} ,$$

giving

$$\sigma(\gamma p \to \phi p) = 610 \pm 35 \pm 170 \text{ nb} ,$$

which is in agreement with a previous measurement on the K^+K^- decay mode in the same photon energy range [7].

The slope, b, of the differential cross-section in the φ mass region can be seen in fig. 12, which gives values of b in 100 MeV bins of $\pi^+\pi^-\pi^0$ mass. The observed mass dependence is consistent with that of $\pi^+\pi^-$ photoproduction [3] and is in general agreement with hadronic diffractive processes [16]. The slope for the φ mass region is $b = -6.9 \pm 0.5$ GeV^{-2} (see table 1).

Table 2 contains some values of spherical harmonic moments of the 3π decay distribution for the ϕ mass range, 0.975-1.065 GeV. The effective contributions to the cross-section from SCHC P-wave states, evaluated, as before, from $\langle Y_2^0 \rangle$ and $\langle \mathrm{Re}\ Y_2^2 \rangle$, are given in table 4. Since previous studies of ϕ meson photoproduction [6,7] have shown that SCHC holds in the production, the agreement seen in table 4 between $\sigma(\gamma p \to \phi p) B(\phi \to \pi^+\pi^-\pi^0)$ and σ_{SCHC} implies that the data correspond to a vector meson, produced conserving s-channel helicity, superposed on a background which is isotropic in the decay angular distribution.

4.3 Production of "$\omega'(1670)$"

Details of the photoproduction of the peak seen in fig. 13 around 1.67 GeV have already been reported [1]. The mass, width, and cross-section, as obtained from an incoherent sum of a Breit-Wigner function and a polynomial background (solid curve in fig. 13) are

$$M = 1.67 \pm 0.02 \text{ GeV}$$

$$\Gamma = 0.16 \pm 0.02 \text{ GeV}$$

$$\sigma B(\pi^+\pi^-\pi^0) = 100 \pm 20 \text{ nb} .$$

The slope, b, of the differential cross-section for the appropriate mass region is seen from fig. 12 to be $b = -2.8 \pm 0.4 \text{ GeV}^{-2}$.

The $\pi^\pm\pi^0$ and $\pi^+\pi^-$ mass spectra for the "ω'" mass range (see fig. 14) indicate that the decay proceeds mainly via $\rho\pi$. The ratio $\rho^+:\rho^-:\rho^0$ is consistent with 1:1:1 as expected for an isoscalar state.

As has been noted [1], the most favoured spin-parity of this state is 1^-, so that it is a candidate for a radial recurrence of either the ω or ϕ meson. The photoproduction cross-section for a ϕ' candidate decaying into $\pi^+\pi^-\pi^0$ would be expected to be less than 20 nb, assuming VDM and ideal mixing, so that the ω' interpretation is favoured on the basis of the observed cross-section of 100 nb. However, this cross-section determination assumed a specific model for the fit to the $\pi^+\pi^-\pi^0$ mass spectrum. Another model, involving a coherent sum of a Breit-Wigner amplitude and a polynomial background, P(m), given by:

$$I(m) = (1 - \alpha)|P(m)|^2 + \left|\sqrt{\alpha}P(m)e^{i\phi} + \beta \frac{\frac{1}{2}\Gamma}{(m - m_R - \frac{1}{2}i\Gamma)}\right|^2 , \qquad (9)$$

gives a reduction of the cross-section to 15 ± 2 nb when the requirement of maximum constructive interference with the $J^P = 1^-$ background is imposed (corresponding to $\alpha \simeq 25\%$, the fraction of $J^P = 1^-$ in the total background, see section 4.5 and ref. 1). The mass and width of the peak are then 1.65 ± 0.02 GeV and 0.12 ± ± 0.01 GeV, respectively. With this cross-section, the peak would be compatible with a ϕ' interpretation, but such coherence with the background is perhaps physically unreasonable. For example the spin configuration of the background is not typically that of an SCHC 1^- state (see section 4.4), whereas maximum interference requires the same spin alignment both of the 3π state and of the recoil proton.

Comparison of diffractive photoproduction of vector mesons with e^+e^- annihilation can be made via the approximate relation

$$\sigma_{peak}(e^+e^- \to V) \simeq \frac{64\pi^2\alpha b}{m_V\Gamma_V} \frac{\sigma(\gamma p \to Vp)}{\sigma^2_{tot}(Vp)} . \qquad (10)$$

For an ω' interpretation of the peak, the values

$$\sigma(\gamma p \to Vp)B(V \to \rho\pi) = 100 \pm 20 \text{ nb} ,$$

$$b = 4.5 \pm 0.3 \text{ GeV}^{-2} ,$$

$$m_V = 1.67 \pm 0.02 \text{ GeV} ,$$

$$\Gamma_V = 0.16 \pm 0.02 \text{ GeV} ,$$

and taking

$$\sigma_{tot}(Vp) = 15 \text{ mb} ,$$

give, via eq. (10),

$$\sigma_{peak}(e^+e^- \to \omega' \to \rho\pi) = 5.2 \pm 1.3 \text{ nb} .$$

A ϕ' interpretation, with

$$\sigma(\gamma p \to Vp) \cdot B(V \to \rho\pi) = 15 \pm 2 \text{ nb} ,$$

$$m_V = 1.64 \pm 0.02 \text{ GeV} ,$$

$$\Gamma_V = 0.12 \pm 0.01 \text{ GeV} ,$$

and

$$\sigma_{tot}(Vp) = 10 \text{ mb} ,$$

gives

$$\sigma_{peak}(e^+e^- \to \phi' \to \rho\pi) = 2.4 \pm 0.7 \text{ nb} .$$

Data from e^+e^- annihilation [17] give an upper limit for the peak cross-section for such a $\rho\pi$ resonance (with mass and width of 1.65 GeV and 0.15 GeV, respectively) of 2.5 nb at the 90% confidence level. Thus the presently available data on $e^+e^- \to \rho\pi$ slightly favour the ϕ' interpretation of the photoproduction results, although it is to be noted that there is considerable uncertainty involved in eq. (10) and in the analysis of the e^+e^- data. A ϕ' state has been reported [17] in e^+e^- annihilations, decaying mainly via K^*K, with a mass and width of 1.68 ± ± 0.01 GeV and 0.18 ± 0.02 GeV respectively, equal, within errors, to the $\pi^+\pi^-\pi^0$ peak observed here. However, in the present experiment, no corresponding K^*K peak is observed [18] where a significant signal would be expected (assuming VDM) from the e^+e^- results. In addition, a broad ω' resonance decaying mainly via $\omega\pi^+\pi^-$ is required in a global fit to the e^+e^- annihilation data [17]. This is not consistent with the ω' interpretation of the narrower $\pi^+\pi^-\pi^0$ peak observed here.

4.4 Production of the 3π continuum

After subtraction of contributions from the three resonances, ω, ϕ, and "$\omega'(1670)$", the cross-section for production of $\pi^+\pi^-\pi^0$ states of masses up to 2 GeV is found to be 2.5 ± 0.5 μb. Considered as a broad peaking in the mass spectrum, the peak mass is about 1.2 GeV and the full width at half maximum about 800 MeV.

(In the following analyses, the contributions of ϕ and "$\omega'(1670)$", which are a small part of the total cross-section, are included.)

Production of these 3π states shows the characteristics of a diffractive mechanism. The cross-section is only weakly dependent on beam energy E_γ across the whole mass range, as shown in fig. 15 and in table 5 which gives values of n from fits of the form, $\sigma(E_\gamma) = \sigma_0 E_\gamma^n$. Also, the slopes b of the t distribution as a function of mass, shown in fig. 12, are typical of diffraction. The 2π mass spectra, shown in fig. 16, indicate ρ meson production, with the ratio $\rho^+:\rho^-:\rho^0 = 1:1:1$ (the reduction in the number of ρ^0 mesons for the highest 3π masses is due to acceptance effects and is completely reproduced by the Monte Carlo simulation). This implies that the $\rho\pi$ system is in an $I^G = 0^-$ state, as expected for diffractive fragmentation of the photon.

The moments $\langle Y_\ell^m(\cos\theta, \phi)\rangle$ have been evaluated for masses up to around 2 GeV and some are shown in fig. 17 in 100 MeV bins of mass. Only the $\langle Y_2^0\rangle$ moment shows any significant deviation from zero outside the resonance regions. There is thus no direct evidence for the presence of 3π states with spin $J > 1$. Dominance of the continuum by $J^P = 1^-$ states produced by an SCHC mechanism is ruled out by the small magnitude of the $\langle Y_2^0\rangle$ signals and their mainly positive sign.

4.5 Spin-parity analysis

To analyse the spin parity of the $\pi^+\pi^-\pi^0$ system as a function of mass, the method of maximum-likelihood fits to the Dalitz plot was used. The decay amplitudes were constructed with the Zemach tensor formalism [19]. This analysis has the advantages that states with different spin parities do not interfere and that the decay mechanism of the 3π systems is separated from the production. However, only the intensities of the contributing partial waves can be measured; no information is available about their phases or production characteristics. (The limited statistics available in photoproduction experiments preclude a full analysis of the Ascoli type [20]).

Since the $\pi^+\pi^-\pi^0$ states are dominated by $\rho\pi$ substates (as seen in fig. 16), consistent with about one ρ meson per event, $\rho\pi$ decay amplitudes were used in the fits to the Dalitz plot. To allow for the inelastic background within the missing

mass squared cut and the possible presence of some non-ρ states, an amplitude corresponding to 3π Lorentz invariant phase space was also included. For completeness, full details of the methods of construction of the amplitudes are given in the Appendix.

Given intensities, $I_{JP}(E_1, E_2)$, where E_1, E_2 are pion energies, the probability density function at event i is

$$f_i(\underset{\sim}{\alpha}) = \sum_{\alpha_{JP}} \{\alpha_{JP} I_{JP} \Big/ \int I_{JP}\, dE_1\, dE_2$$

where α_{JP} is the fraction of spin parity J^P in the data. Then the negative log likelihood function to be minimized is

$$L(\underset{\sim}{\alpha}) = -\sum_i \log f_i(\underset{\sim}{\alpha})$$

with the summation over all events in a given interval of $\pi^+\pi^-\pi^0$ mass. The integrals over the Dalitz plot were performed by the Monte Carlo method using only simulated events which fell within the acceptance aperture of the apparatus and were reconstructed by the software. Smearing of momenta due to resolution effects was accounted for, and the same cuts were applied to both the data and the Monte Carlo events. The fits were made, using the program MINUIT [21] in 100 MeV bins of 3π mass with the following intensities allowed to contribute: 3π phase space, ρπ phase space*), $J^P = 0^-$ ρπ, 1^- ρπ, 1^+ ρπ, 2^- ρπ, 2^+ ρπ, and 3^- ρπ. In the initial exploratory fits, the intensities of all J^P states with $J > 1$ were found to be small for all $\pi^+\pi^-\pi^0$ mass bins up to 2 GeV. This is consistent with the moments analysis described in section 4.4. Accordingly, these contributions were set to zero for all subsequent fits. The states 1^+ (S-wave) ρπ and 1^+ (D-wave) ρπ can interfere in the fits and such interference terms were taken into account (imposing relatively real phase). The resulting cross-sections for the production of the various contributions are shown in fig. 18; the errors correspond to those given by the program MINUIT. The most obvious features of the results are the almost constant

*) The intensity for ρπ phase space was the sum of the separate intensities of $\rho^+\pi^-$, $\rho^-\pi^+$, and $\rho^0\pi^0$.

fraction of 3π and $\rho\pi$ phase space (the "background") with mass, the rapid fall in the intensity of $J^P = 1^-$ as a fraction of the total above the ω meson mass, and the peaking in the $J^P = 1^+$ intensity around a mass of 1.2 GeV. This peaking could be due partly to production of the H meson, the iscoscalar partner of the well-established B meson; only one experiment has so far produced evidence for the H meson [22], giving a mass and width of 1.19 ± 0.06 GeV and 0.32 ± 0.05 GeV, respectively, with some uncertainty in these values due to their model dependency. Recent data [23] indicate that the B meson could be seen in photoproduction so that, assuming simple VDM, the H meson would also be expected to be observed. Diffractive photoproduction of $\rho\pi$ via the one-pion exchange Deck mechanism, which would populate the $J^P = 1^+$ $\rho\pi$ decay state, should be relatively unimportant in reaction (1) owing to the small $\rho \to \pi\gamma$ radiative width (for the same reason, one-pion-exchange does not contribute to ρ^0 photoproduction). As the contribution to the total 1^+S $\rho\pi$ intensity from the Deck term in $\pi^-\rho \to \rho\pi p$ is about 20 μb at these energies [24], the contribution in photoproduction can be calculated to be (in the limit $M_\gamma \approx M_\pi$) about 10 nb, using [25] $\Gamma(\rho \to \pi\gamma)/\Gamma(\rho \to \pi\pi) = 4.4 \times 10^{-4}$. Since the data of ref. 22 suggest that only S-wave contributes to the $H \to \rho\pi$ decay, the fits were repeated with separate 1^+ S-wave and D-wave intensities (in fact, the D/S-wave ratio was found to be poorly constrained in the earlier fits). The resulting intensities (for $J^P = 1^+$ only) are shown in fig. 19, and now indicate a narrower peak in the 1^+ S-wave $\rho\pi$ intensity with mass and width of about 1.05 GeV and 200 MeV, produced with a total cross-section of about 300 nb. The smaller D-wave contribution peaks at a higher mass. Thus, it is possible that H meson production is a major contribution to the $J^{PC} = 1^{+-}$ $\rho\pi$ enhancement seen in this experiment, although the resonant nature of the enhancement has not been established.

5. CONCLUSIONS

Several processes contribute to diffractive photoproduction of $\pi^+\pi^-\pi^0$ at photon energies in the range 20-70 GeV. The ω meson is produced with a cross-section of 1010 nb which does not vary with photon momentum, and the production is peripheral; a

fit to dN/dt = a exp (bt) yields (averaging over the photon energy range) a slope b of $-7.3\ \text{GeV}^{-2}$. The spin-density matrix elements of the ω have been evaluated from the moments of the decay angular distribution in the s-channel helicity system. These show that the production proceeds dominantly via natural parity exchange and conserves s-channel helicity.

The ϕ meson is observed in its 3π decay mode with $\sigma(\gamma p \to \phi p) \cdot B(\phi \to \pi^+\pi^-\pi^0) = 90 \pm 5 \pm 25$ nb, and is observed in the mass spectrum on a substantial background. Analysis of the decay distributions shows that, for the background being isotropic, ϕ photoproduction conserves s-channel helicity.

A peak is observed at a mass of 1.67 GeV with width 160 MeV. With the assumption that there is no interference with the background, the cross-section times branching ratio to $\pi^+\pi^-\pi^0$ is 100 nb. In the extreme case of maximum interference with the background, σB could be as low as 15 nb. This complicates the interpretation of the peak in terms of a vector meson recurrence since it could be due to either, or both, of the expected isoscalar ω' and ϕ' states. The simplest interpretation is, however, that the peak is due to a major decay mode of an ω' radial recurrence of the $\omega(783)$.

In addition to these three peaks, the mass spectrum shows a broad continuum of 3π states corresponding to a total production cross-section of 2.5 μb. An analysis of the moments of the decay angular distributions shows no evidence of states with spin greater than J = 1, and indicates that production of $J^{PC} = 1^{--}$ states by s-channel helicity conservation is not an important mechanism away from the ω and ϕ resonances. These 3π states are found to arise almost wholly from $\rho\pi$ production. An analysis of the Dalitz plot in terms of $\rho\pi$ decay amplitudes indicates that states with $J^{PC} = 1^{--}$ make up less than half of the $\pi^+\pi^-\pi^0$ mass spectrum above the ω meson mass. In addition, this analysis shows an enhancement in the $J^{PC} = 1^{+-}$ partial wave consistent with production of the H(1190) meson with a total photoproduction cross-section, $\sigma(\gamma p \to Hp)B(H \to \rho\pi)$, of about 300 nb.

Acknowledgements

We are grateful to the Omega group at CERN for their help in maintaining and running the spectrometer and providing on-line and off-line software. The work of the technical support staff in our home institutions, and the support at the computer centres at the Rutherford Appleton Laboratory, CERN, and the RHRZ at Bonn have been invaluable. We thank the SERC (UK), the BMFT (Fed. Rep. Germany), and the IN2P3 (France) for financial support.

REFERENCES

[1] M. Atkinson et al., preprint CERN-EP/83-27 (1983), to be published in Phys. Lett. B.

[2] J. Ballam et al., Phys. Rev. D 7 (1973) 3150.

[3] D. Aston et al., Nucl. Phys. B209 (1982) 56.

[4] R.M. Egloff et al., Phys. Rev. Lett. 43 (1979) 1545.

[5] A.M. Breakstone et al., Phys. Rev. Lett. 47 (1981) 1782.

[6] R.M. Egloff et al., Phys. Rev. Lett. 43 (1979) 657.

[7] D. Aston et al., Nucl. Phys. B172 (1980) 1.

[8] D. Aston et al., Nucl. Instrum. Methods 197 (1982) 287.

[9] P.J. Bussey et al., preprint CERN-EP/82-186 (1982), to be published in Nucl. Instrum. Methods.

[10] Experiments at CERN in 1980 (CERN, Geneva, 1980).

[11] J.-C. Lassalle, F. Carena and S. Pensotti, Nucl. Instrum. Methods 176 (1980) 371.

[12] J. Friedman, SAGE Reference Manual, SLAC Computation Group Technical Memo 145 (1972).

[13] K. Schilling et al., Nucl. Phys. B15 (1970) 397.

[14] A.P. Waite, MAP Program Guide (1981), University of Manchester, unpublished.

[15] See T.H. Bauer et al., Rev. Mod. Phys. 50 (1978) 261, for a review.

[16] U. Amaldi et al., Rev. Nucl. Sci. 26 (1976) 365.

[17] J. Buon et al., Phys. Lett. 118B (1982) 221.

[18] M. Atkinson et al., "Photoproduction of $K\bar{K}\pi$ final states in the energy range 20-70 GeV", to be submitted to Nucl. Phys. B.

[19] C. Zemach, Phys. Rev. B140 (1965) 97.

[20] J.D. Hansen et al., Nucl. Phys. B81 (1974) 403.

[21] CERN Computer Centre, Long Write Up D506/516 (1977).

[22] J.A. Dankowitch et al., Phys. Rev. D 46 (1981) 581.

[23] M. Atkinson et al., preprint CERN-EP/81-113 (1981).

[24] C. Daum et al., Nucl. Phys. B182 (1981) 269.

[25] Review of Particle Properties, Phys. Lett. 111B (1982).

Table 1

Results of fits of the differential cross-sections to the forms a exp $(bt + ct^2)$ and a exp (bt)

3π mass range (GeV)	E_γ range (GeV)	$\|t\|$ range (GeV^2)	b (GeV^{-2})	c (GeV^{-4})	$\frac{d\sigma}{dt}\|_{t=0}$ ($\mu b/GeV^2$)
0.72-0.86 (ω range)	20-30	0.04-0.4	-7.2 ± 0.3	-	7.3 ± 0.3
		0.04-0.8	-9.5 ± 0.1	4.4 ± 0.2	-
	30-45	0.04-0.4	-7.4 ± 0.2	-	7.5 ± 0.3
		0.04-0.8	-8.8 ± 0.6	2.8 ± 0.9	-
	45-70	0.04-0.4	-7.2 ± 0.9	-	7.3 ± 0.9
		0.04-0.8	-8.7 ± 1.9	1.6 ± 3.3	-
0.975-1.065 (ϕ range)	20-70	0.04-0.4	-6.9 ± 0.5	-	-
1.5-1.86	20-70	0.04-0.4	-2.8 ± 0.4	-	-

Table 2

Normalized moments of the $\pi^+\pi^-\pi^0$ decay distribution in the helicity system (for the ω range, the angles used are θ and ψ; for the other ranges, θ and ϕ are used)

	$\pi^+\pi^-\pi^0$ mass range (GeV)		
	0.72-0.84 (ω range) $0.02 < -t < 0.4$ GeV^2	0.975-1.065 (ϕ range) $0.02 < -t < 1.0$ GeV^2	1.5-1.84 ("ω'" range) $0.02 < -t < 1.0$ GeV^2
Y_1^0	0.025 ± 0.018	-0.018 ± 0.032	-0.009 ± 0.026
Re Y_1^1	0.009 ± 0.027	-0.025 ± 0.036	0.021 ± 0.026
Y_2^0	-0.358 ± 0.022	-0.067 ± 0.034	0.143 ± 0.027
Re Y_2^1	0.046 ± 0.023	0.067 ± 0.033	-0.027 ± 0.026
Im Y_2^1	-0.053 ± 0.020	0.027 ± 0.034	0.068 ± 0.026
Re Y_2^2	0.209 ± 0.027	0.057 ± 0.035	0.071 ± 0.025
Im Y_2^2	0.045 ± 0.027	-0.026 ± 0.037	-0.007 ± 0.025
Y_3^0	-0.027 ± 0.020	0.022 ± 0.034	0.015 ± 0.026
Y_4^0	-0.012 ± 0.021	0.021 ± 0.033	0.007 ± 0.026
Y_6^0	-0.009 ± 0.021	0.014 ± 0.033	-0.044 ± 0.026

Table 3

Spin density matrix elements, in the helicity frame, for the ω mass region, 0.72-0.84 GeV, evaluated by the method of moments

$\rho^{\alpha}_{mm'}$	Measured value
ρ^{0}_{00}	0.052 ± 0.015
Re ρ^{0}_{10}	0.037 ± 0.009
ρ^{0}_{1-1}	0.027 ± 0.012
ρ^{1}_{11}	0.005 ± 0.040
ρ^{1}_{00}	0.027 ± 0.063
Re ρ^{1}_{10}	-0.075 ± 0.035
ρ^{1}_{1-1}	0.426 ± 0.062
Im ρ^{2}_{10}	-0.100 ± 0.035
Im ρ^{2}_{1-1}	-0.401 ± 0.061

Table 4

Cross-sections (nb) for production of SCHC P-wave states evaluated as described in the text (only statistical errors are given)

	$\pi^+\pi^-\pi^0$ mass range (GeV)	
	0.72-0.86 (ω region)	0.975-1.065 (ϕ region)
$-\sqrt{20\pi}\sum Y_2^0(\theta)$	830 ± 50	1200 ± 600
$\frac{1}{P_\gamma}\sqrt{\frac{40\pi}{3}}\sum \mathrm{Re}\, Y_2^2(\theta,\psi)$	930 ± 120	775 ± 230
Fit to the mass spectrum	1010 ± 15	610 ± 35

Table 5

Results of fits to the energy dependence of the total cross-sections, $\sigma(\gamma p \to \pi^+\pi^-\pi^0 p)$, for several ranges of 3π mass. The parametrization used for $\sigma(E_\gamma) = \sigma_0 E_\gamma^n$

3π mass range (GeV)	n
0.72-0.84	-0.12 ± 0.09
1.00-1.20	-0.01 ± 0.10
1.20-1.50	-0.28 ± 0.09
1.50-1.80	-0.25 ± 0.11
1.80-2.20	-0.58 ± 0.13

APPENDIX

CONSTRUCTION OF $\rho\pi$ DECAY AMPLITUDES

In the Zemach formalism the amplitude for the two-step decay of a parent state X of spin J:

$$X \to \rho\pi \text{ with relative angular momentum } L ,$$

$$\rho \to \pi\pi \text{ with relative angular momentum } \ell = 1 ,$$

is a traceless, symmetric tensor of rank J in Cartesian 3-space. This tensor is to be constructed from the two pure tensors, of ranks L and ℓ, describing the decay steps, which are constructed from the particle momenta. The combination of these two tensors yields a tensor of rank $(L + \ell)$, which can be reduced to tensors of ranks $(L + \ell - 2)$, $(L + \ell - 4)$, etc., by repeated contraction over pairs of indices; alternatively, tensors of ranks $(L + \ell - 1)$, $(L + \ell - 3)$, etc., can be obtained by application of the totally antisymmetric symbol and contraction over pairs of indices.

To illustrate these procedures, the tensor amplitudes for $J^P = 1^+$ (D-wave) and $J^P = 2^+$ are derived below.

a) $J^P = 1^+$ (D-wave) $\rho\pi$ ($L = 2$, $\ell = 1$). (See fig. 20 for definitions of the momenta $\underset{\sim}{p}$, $\underset{\sim}{q}$.) The tensor describing the ρ decay is just $\underset{\sim}{q}$. The rank-2 tensor describing the D-wave $\rho\pi$ decay is $p_i p_j$ [a tensor is written conventionally as its (i,j)th component]; this has to be made symmetric and traceless, giving $(p_i p_j - \frac{1}{3}\underset{\sim}{p}^2\delta_{ij})$. These two tensors are combined to get the raw rank-3 tensor $(p_i p_j q_k - \frac{1}{3}\underset{\sim}{p}^2\delta_{ij}q_k)$, which is then contracted over the indices (j,k) to give the rank-1 tensor, $\underset{\sim}{p}(\underset{\sim}{p}\cdot\underset{\sim}{q}) - \frac{1}{3}\underset{\sim}{p}^2\underset{\sim}{q}$. The ρ-meson resonance is introduced as a Watson final-state interaction factor so that the amplitude is then

$$\left\{\underset{\sim}{p}(\underset{\sim}{p}\cdot\underset{\sim}{q}) - \tfrac{1}{3}\underset{\sim}{p}^2\underset{\sim}{q}\right\}\frac{\sin\delta\, e^{i\delta}}{q^3} ,$$

where δ are P-wave $\pi\pi$ phase shifts, and there is an extra factor of q in the denominator to cancel the barrier penetration factor of q already present in the tensor amplitude. Finally, the overall decay amplitude is obtained by symmetrizing this, summing over the three ρ meson identifications to get:

$$\underset{\sim}{T}_{1_D^+} = \sum_{\substack{i,j,k \\ \text{cyclic}}} \left\{ \underset{\sim}{p}^i (\underset{\sim}{p}^i \cdot \underset{\sim}{q}^{jk}) - \frac{1}{3} (\underset{\sim}{p}^i)^2 \underset{\sim}{q}^{jk} \right\} \frac{\sin \delta^{jk} \, e^{i\delta^{jk}}}{(q^{jk})^3} .$$

b) $J^P = 2^+$ $\rho\pi$ (L = 2, ℓ = 1). As in case (a), the raw rank-3 tensor is $(p_i p_j q_k - \frac{1}{3} \underset{\sim}{p}^2 \delta_{ij} q_k)$, but now a tensor of rank 2 is required. The anti-symmetric symbol is applied giving $(\varepsilon^{\ell jk} p_i p_j q_k - \frac{1}{3} p^2 \varepsilon^{\ell jk} \delta_{ij} q_k)$ which, after contraction over the indices (j, k) becomes $p_i (\underset{\sim}{p} \times \underset{\sim}{q})_k - \frac{1}{3} \underset{\sim}{p}^2 \varepsilon^{\ell jk} \delta_{ij} q_k$ (the second term is reduced no further algebraically). This is a raw tensor which is to be made symmetric and traceless, multiplied by the ρ-meson resonance term and summed over the three ρ identifications.

Given a complex amplitude which is a tensor of rank J, the intensity on the Dalitz plot is then obtained by combining the tensor with its complex conjugate and repeatedly contracting to obtain a scalar. For example, for a rank-3 tensor, T_{ijk}, the intensity is

$$I = \sum_{i=1,3} \left[\sum_{j=1,3} \left(\sum_{k=1,3} T_{ijk} T^*_{kji} \right) \right] .$$

Figure captions

Fig. 1 : a) Distribution of incident photon energy versus polarization intensity.
b) Photon energy spectrum.
c) Polarization intensity spectrum.

Fig. 2 : Layout of the Ω' spectrometer as equipped for this experiment.

Fig. 3 : Missing mass squared recoiling against the $\pi^+\pi^-\pi^0$ system.

Fig. 4 : Mass spectrum of $\gamma\gamma$ for the reaction $\gamma p \to \pi^+\pi^-\gamma\gamma p$.

Fig. 5 : Mass spectrum of $\pi^+\pi^-\pi^0$. The curve shows the overall acceptance.

Fig. 6 : Definition of the angles used to study the $\pi^+\pi^-\pi^0$ [2] ($\underline{n}$ is the normal to the decay plane spanned by $\pi^+\pi^-\pi^0$).

Fig. 7 : Mass spectrum of $\pi^+\pi^-\pi^0$ in the ω region. The solid curve is from the Monte Carlo simulation, and the dashed curve shows the background required to enable the simulation to reproduce the data well.

Fig. 8 : Cross-section for ω photoproduction as a function of beam energy. The curve shows a fit to the form $\sigma = \sigma_0 E_\gamma^n$ with $n = -0.12 \pm 0.09$. (In addition to the errors shown, there is an overall systematic error of 25%.)

Fig. 9 : $dN(\gamma p \to \omega p)/dt$, corrected for acceptance, for three ranges of photon energy:
a) $20 < E_\gamma < 30$ GeV,
b) $30 < E_\gamma < 45$ GeV,
c) $45 < E_\gamma < 70$ GeV.
The curves show the fits of the form $\exp(bt + ct^2)$, see table 1.

Fig. 10 : a) Distribution of $\cos\theta$ for ω decay, corrected for acceptance. The curve shows a $\sin^2\theta$ distribution.
b) Distribution of $\psi = \phi - \Phi$ for ω decay. The curve shows the form $1 + P_\gamma \cos 2\psi$.

Fig. 11 : Mass spectrum of $\pi^+\pi^-\pi^0$ in the ϕ mass region.

Fig. 12 : Slope, b, of the differential cross-section $d\sigma(\gamma p \to \pi^+\pi^-\pi^0 p)/dt$ fitted to a exp (bt) as a function of $\pi^+\pi^-\pi^0$ mass.

Fig. 13 : Mass spectrum of $\pi^+\pi^-\pi^0$ in the "$\omega'(1670)$" region; the full curve shows a fit to a Breit-Wigner function plus an incoherent polynomial background, and the dashed curve shows the background.

Fig. 14 : 2π mass spectra for $1.6 < M_{3\pi} < 1.75$ GeV:

a) $\pi^+\pi^-$ mass;

b) $\pi^+\pi^0$ mass;

c) $\pi^-\pi^0$ mass.

Fig. 15 : Total cross-section for $\gamma p \to \pi^+\pi^-\pi^0 p$ as a function of beam energy E_γ for

a) $1.0 < M_{3\pi} < 1.2$ GeV,

b) $1.2 < M_{3\pi} < 1.5$ GeV,

c) $1.5 < M_{3\pi} < 1.8$ GeV,

d) $1.8 < M_{3\pi} < 2.2$ GeV.

The curves are from fits to the form $\sigma(E_\gamma) = \sigma_0 E_\gamma^n$, with the values of n given in table 5.

Fig. 16 : 2π mass spectra for the $\pi^+\pi^-\pi^0$ mass ranges:

a) $1.0 < M_{3\pi} < 1.3$ GeV;

b) $1.3 < M_{3\pi} < 1.6$ GeV;

c) $1.6 < M_{3\pi} < 2.0$ GeV.

Fig. 17 : Normalized spherical harmonic moments of the 3π decay distribution as functions of 3π mass.

Fig. 18 : Cross-sections for production of various spin-parity states as determined by maximum likelihood fit.

Fig. 19 : Cross-sections for production of S-wave and D-wave 1^+ $\rho\pi$ states assuming no interference.

Fig. 20 : Definitions of parameters used to construct the Zemach amplitudes.

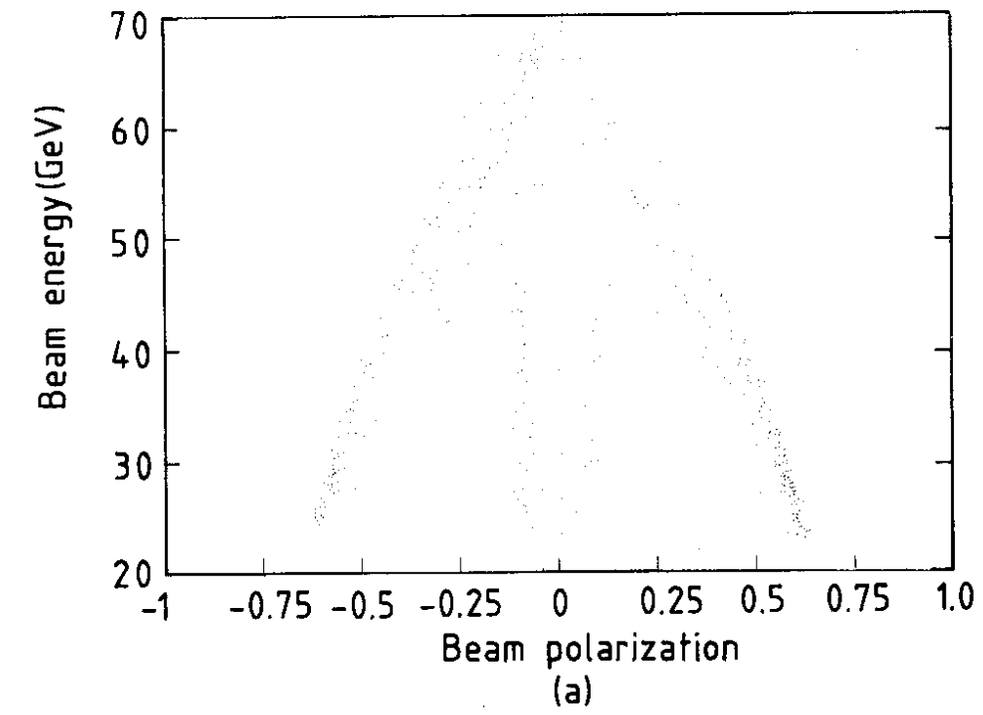
Beam energy(GeV)
70
60
50
40
30
20
-1
-0.75
-0.5
-0.25
0
0.25
0.5
0.75
1.0
Beam polarization
(a)

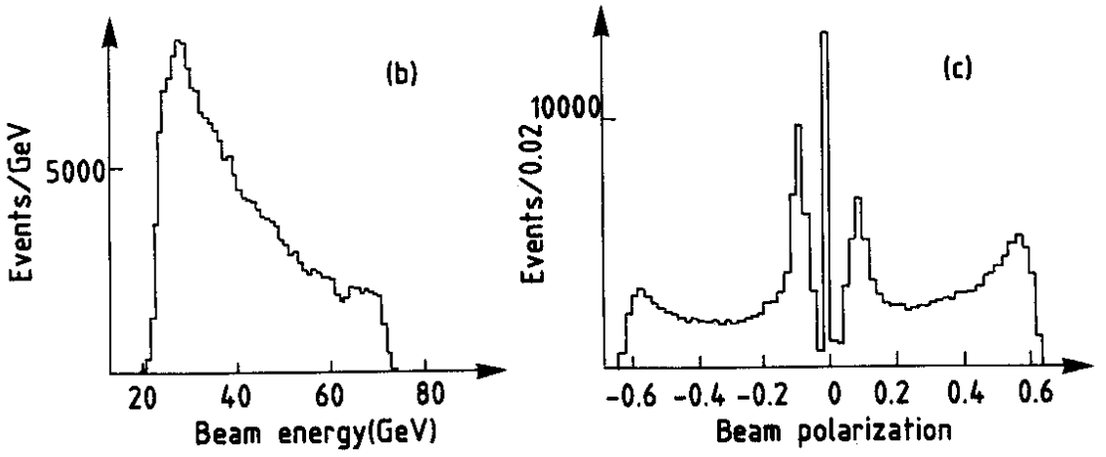
Events/GeV
5000
(b)
20
40
60
80
Beam energy(GeV)
Events/0.02
10000
(c)
-0.6
-0.4
-0.2
0
0.2
0.4
0.6
Beam polarization

Fig. 1

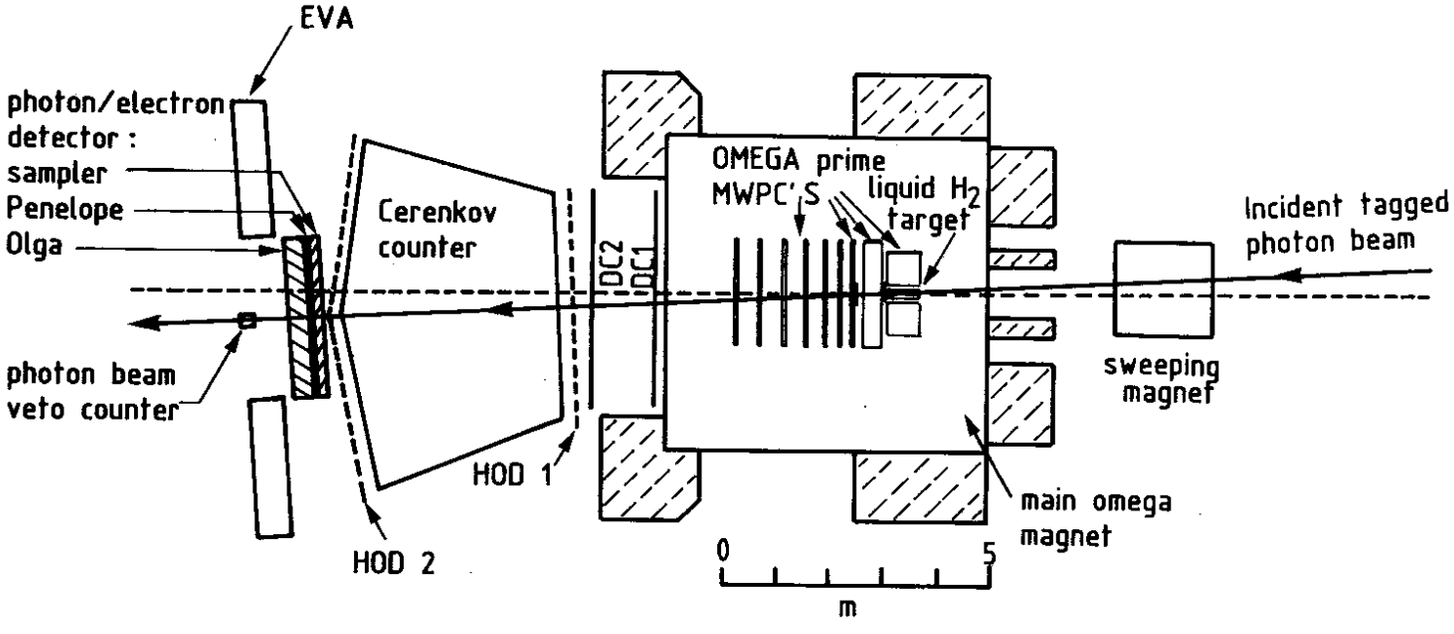
EVA
photon/electron
detector :
sampler
Penelope
Olga
photon beam
veto counter
Cerenkov
counter
DC2
DC1
HOD 1
HOD 2
OMEGA prime
MWPC'S
liquid H_2
target
Incident tagged
photon beam
sweeping
magnef
main omega
magnet
0
5
m

Fig. 2

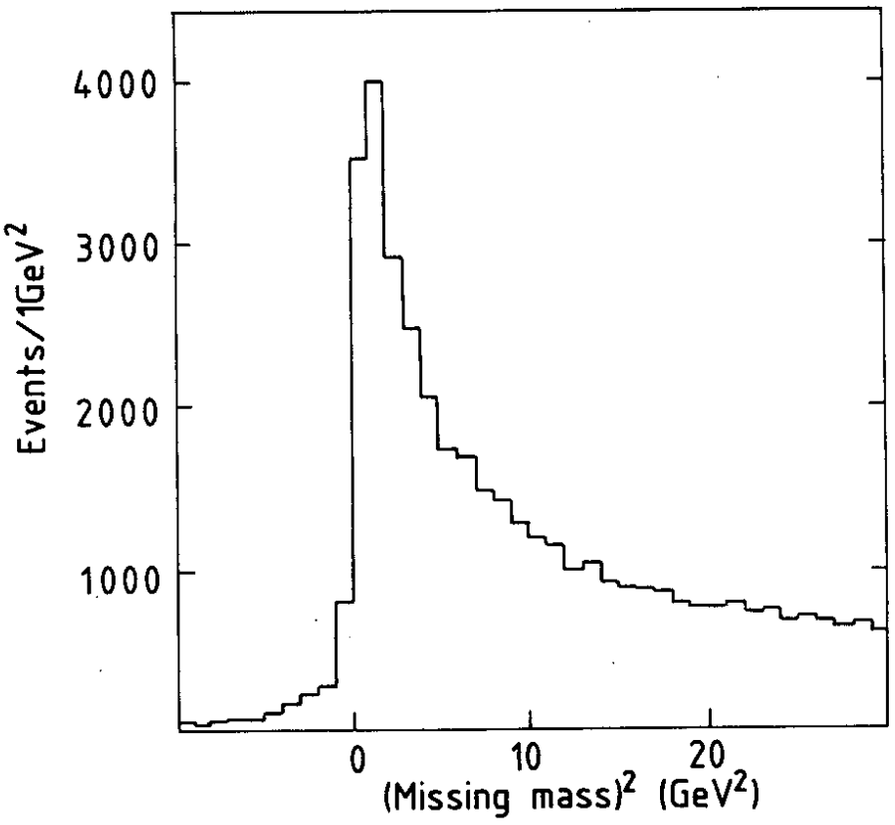
4000
3000
2000
1000
Events/1GeV^2
0
10
20
(Missing mass)^2 (GeV^2)

Fig. 3

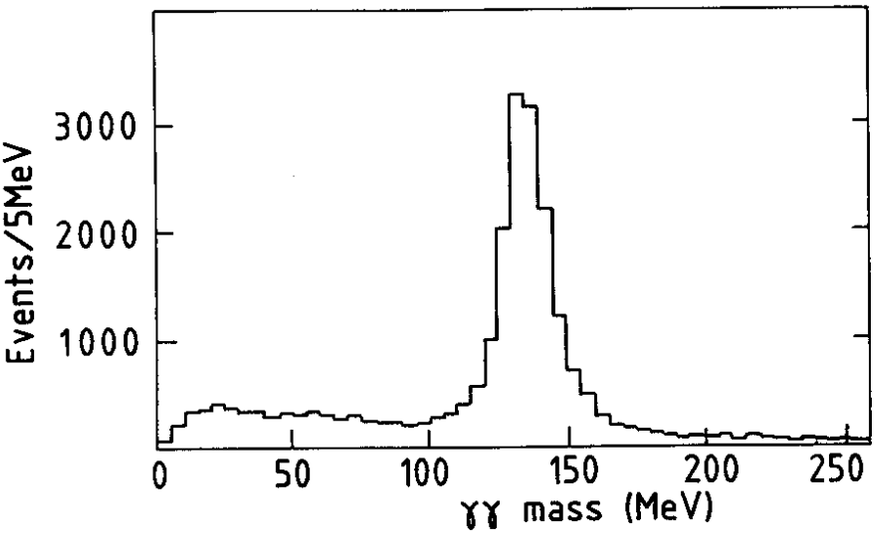
3000
2000
1000
Events/5MeV
0
50
100
150
200
250
$\gamma\gamma$ mass (MeV)

Fig. 4

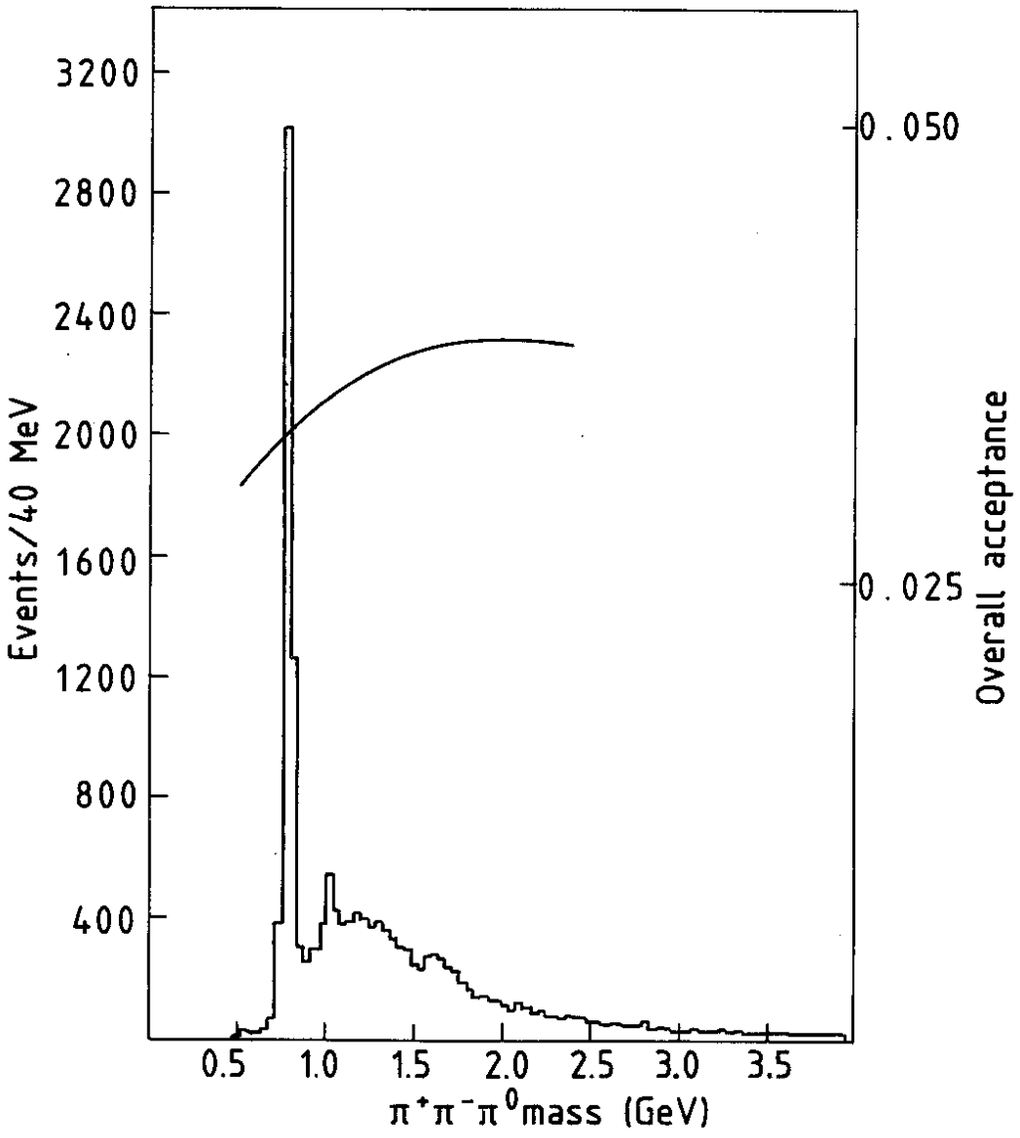
3200
2800
2400
2000
1600
1200
800
400
Events/40 MeV
0.050
0.025
Overall acceptance
0.5
1.0
1.5
2.0
2.5
3.0
3.5
π⁺π⁻π⁰mass (GeV)

Fig. 5

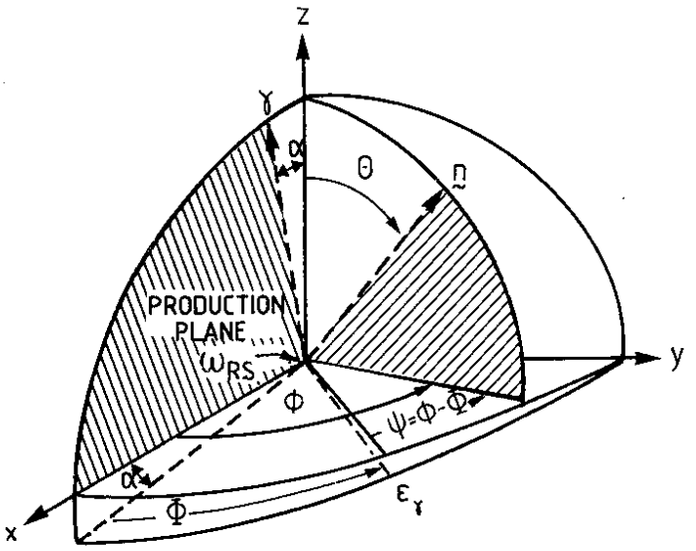

Fig. 6

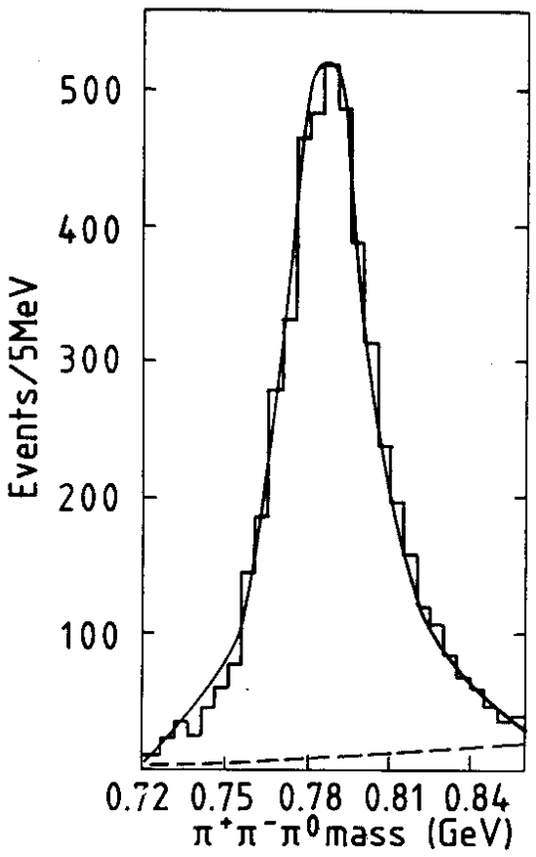
500
400
300
200
100
Events/5MeV
0.72 0.75 0.78 0.81 0.84
$\pi^+\pi^-\pi^0$ mass (GeV)

Fig. 7

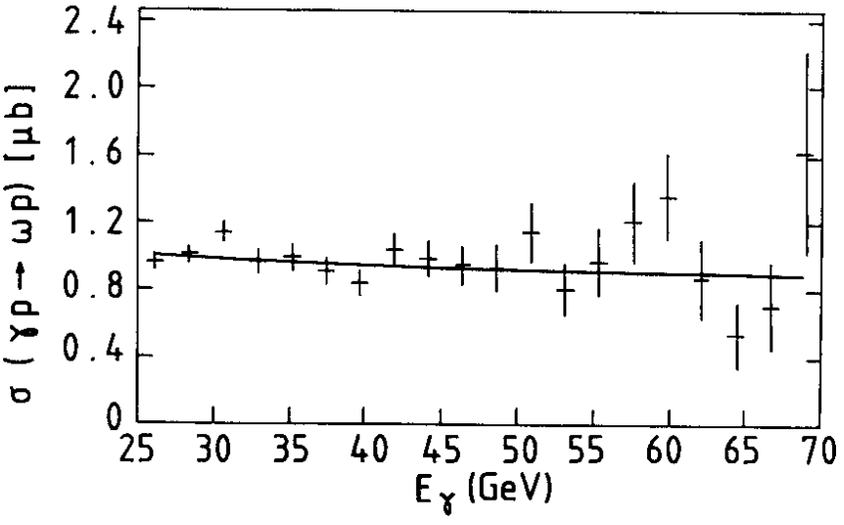
2.4
2.0
1.6
1.2
0.8
0.4
0
$\sigma(\gamma p \to \omega p)$ [μb]
25 30 35 40 45 50 55 60 65 70
E_γ (GeV)

Fig. 8

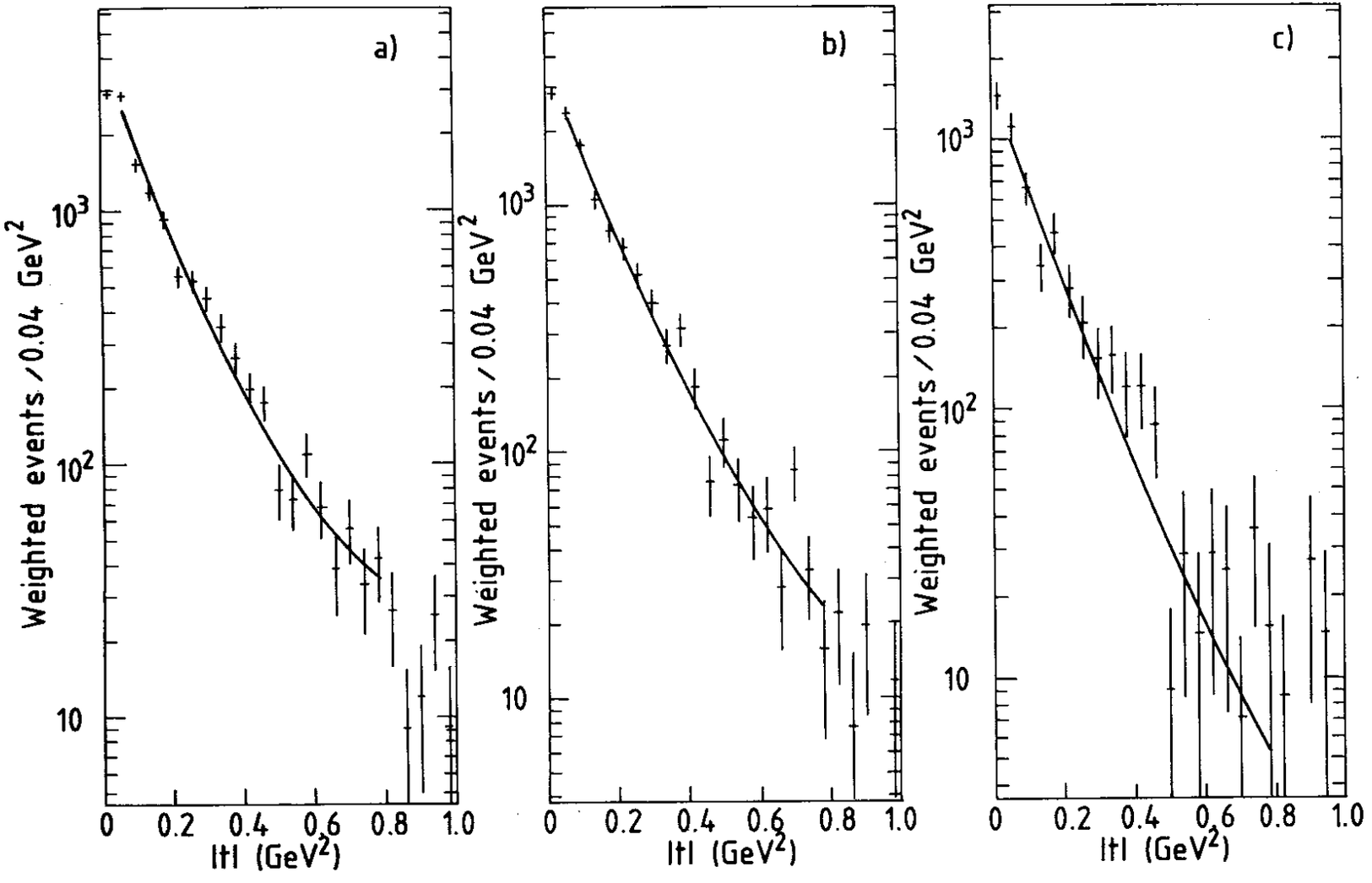

Fig. 9

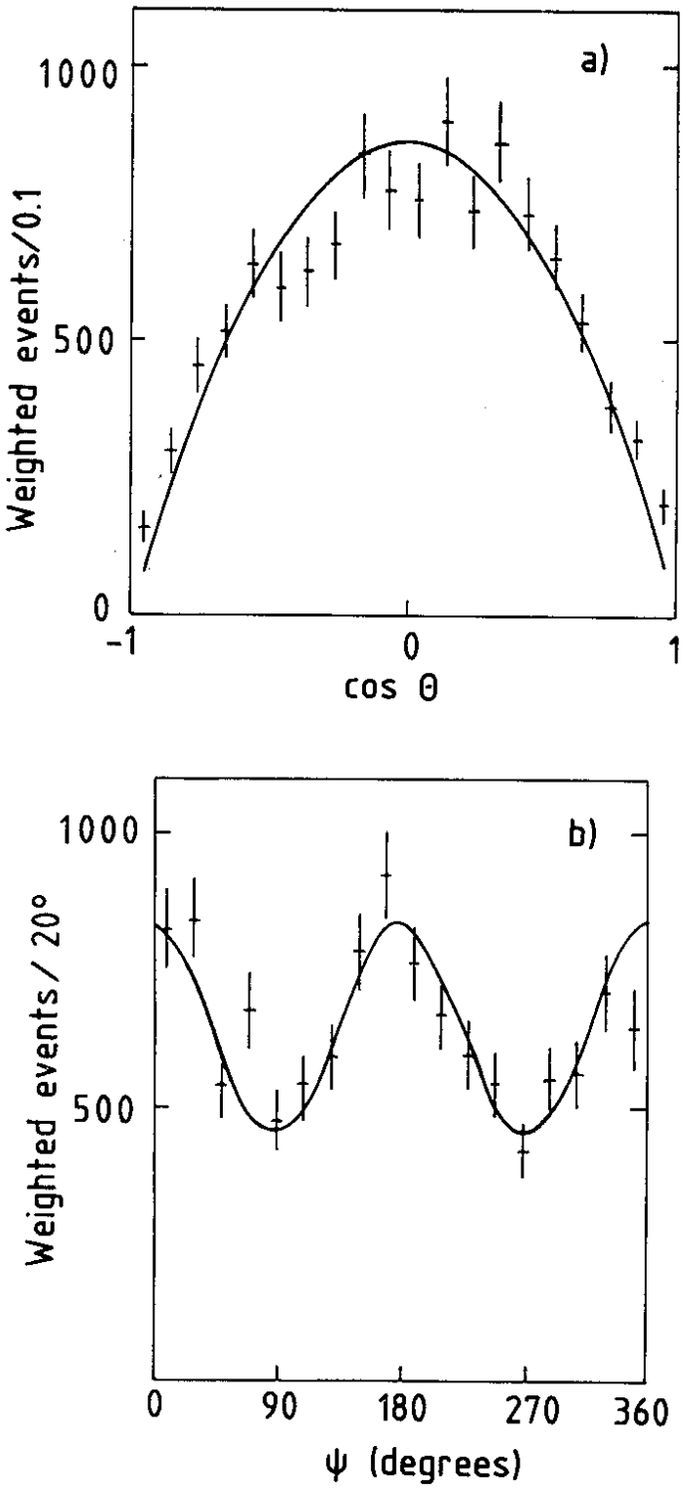
a)
1000
500
0
Weighted events/0.1
-1
0
1
cos θ
b)
1000
500
Weighted events / 20°
0
90
180
270
360
ψ (degrees)

Fig. 10

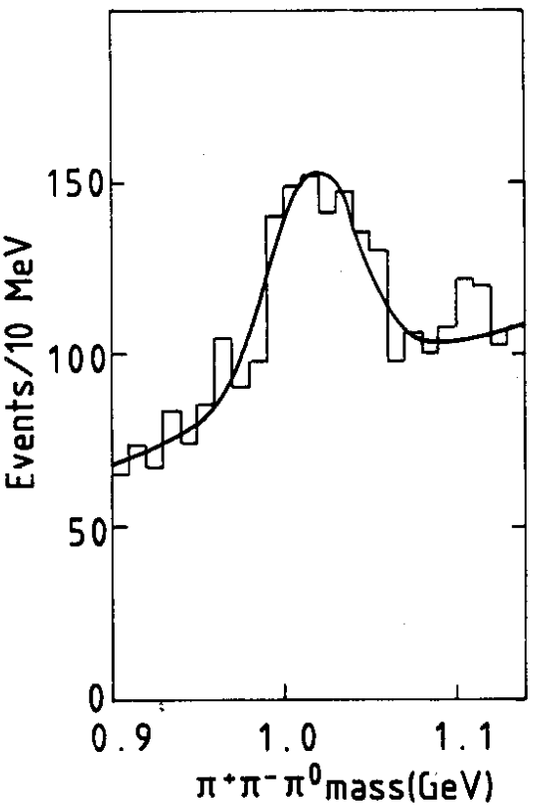
Events/10 MeV
150
100
50
0
0.9
1.0
1.1
π⁺π⁻π⁰mass(GeV)

Fig. 11

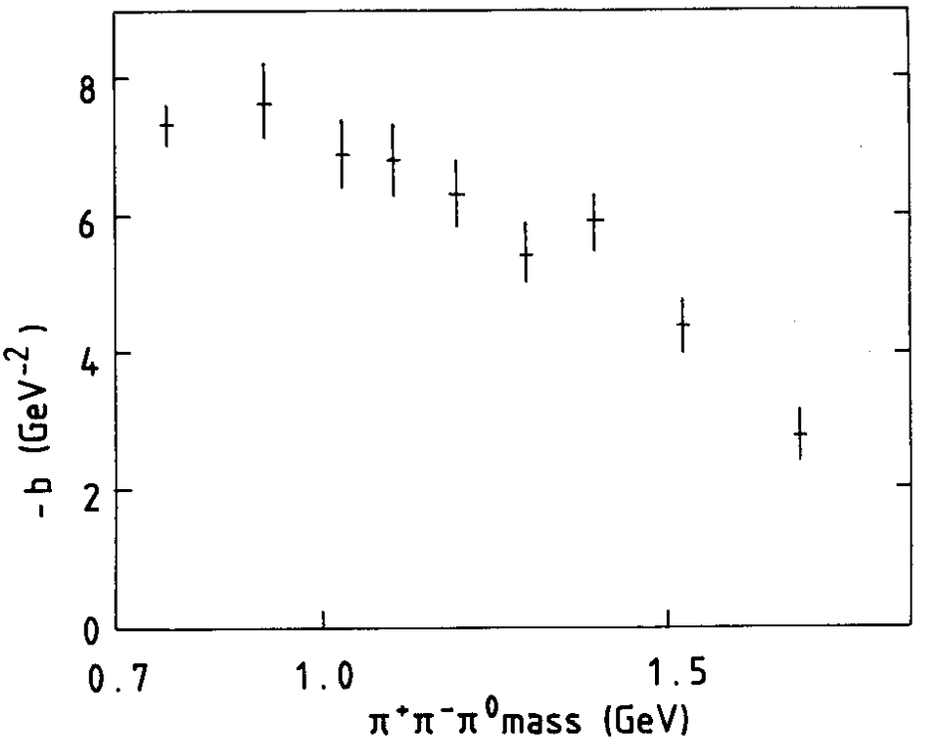
-b (GeV⁻²)
8
6
4
2
0
0.7
1.0
1.5
π⁺π⁻π⁰mass (GeV)

Fig. 12

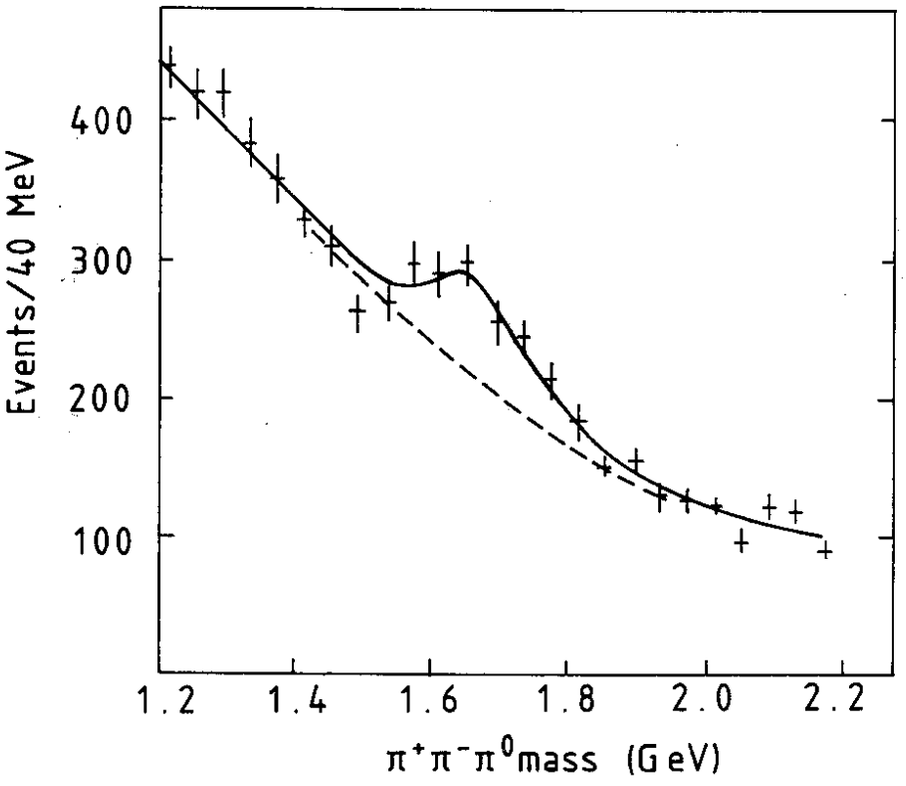
Events/40 MeV
400
300
200
100
1.2
1.4
1.6
1.8
2.0
2.2
π⁺π⁻π⁰mass (GeV)

Fig. 13

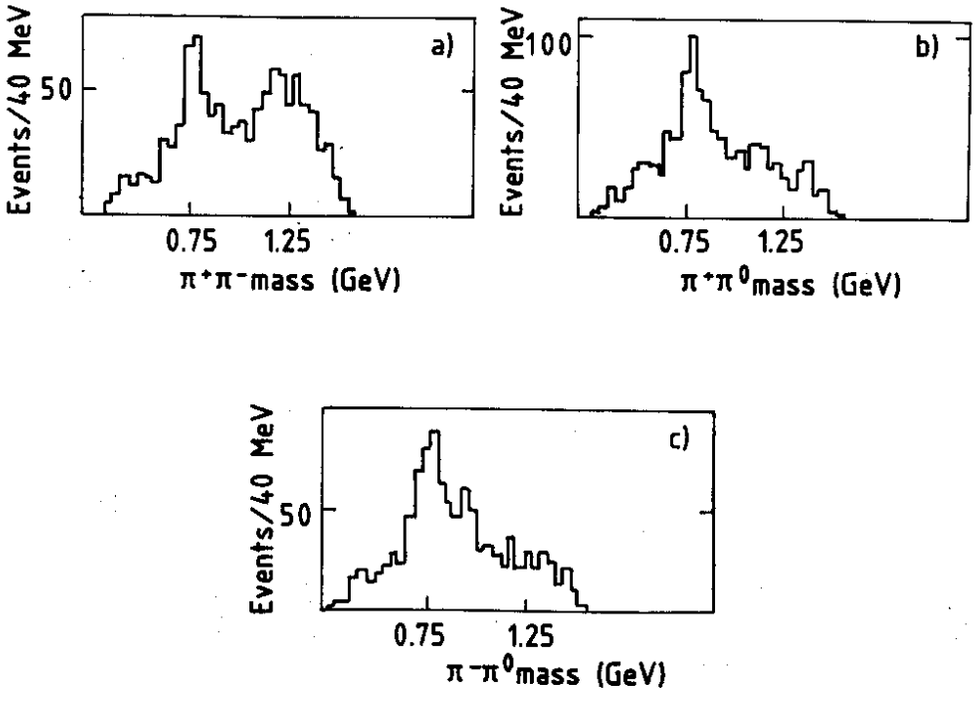
Events/40 MeV
50
a)
0.75
1.25
π⁺π⁻mass (GeV)
Events/40 MeV
100
b)
0.75
1.25
π⁺π⁰mass (GeV)
Events/40 MeV
50
c)
0.75
1.25
π⁻π⁰mass (GeV)

Fig. 14

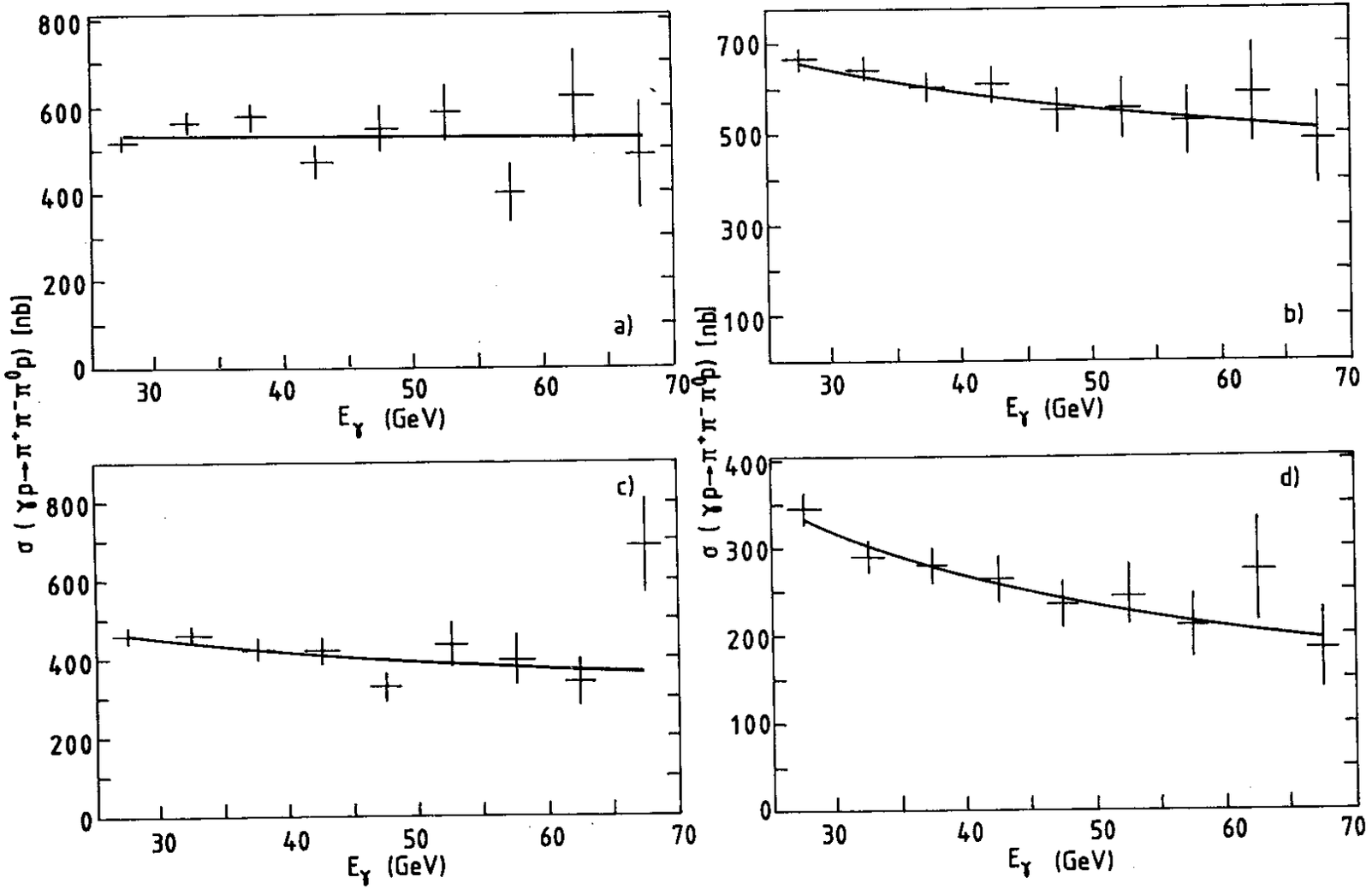

Fig. 15

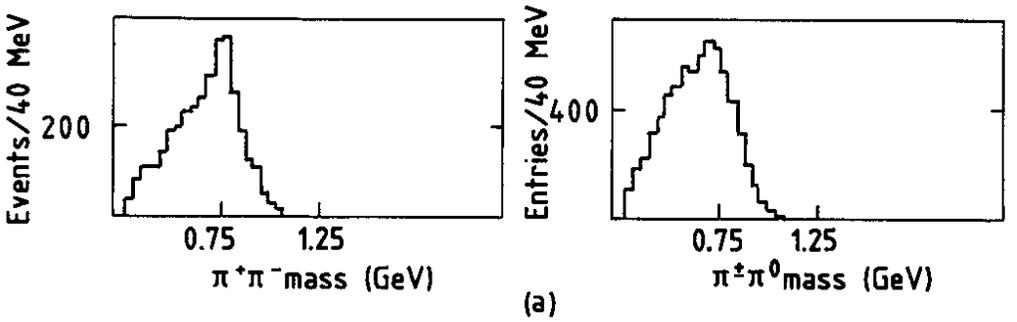
Events/40 MeV
200
0.75
1.25
π⁺π⁻mass (GeV)
Entries/40 MeV
400
0.75
1.25
π±π⁰mass (GeV)

(a)

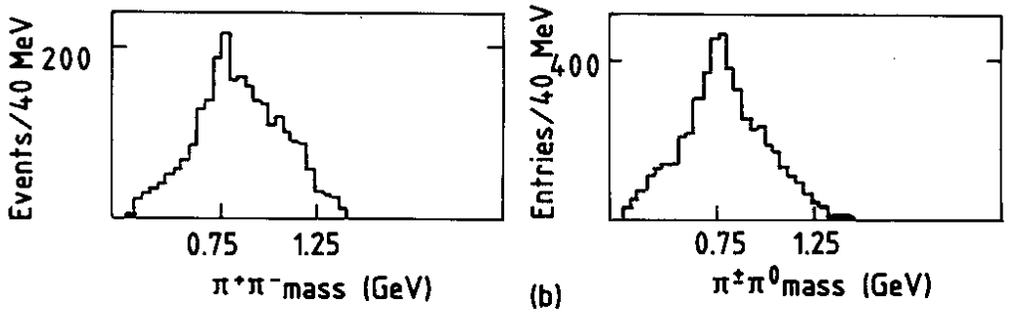
Events/40 MeV
200
0.75
1.25
π⁺π⁻mass (GeV)
Entries/40 MeV
400
0.75
1.25
π±π⁰mass (GeV)

(b)

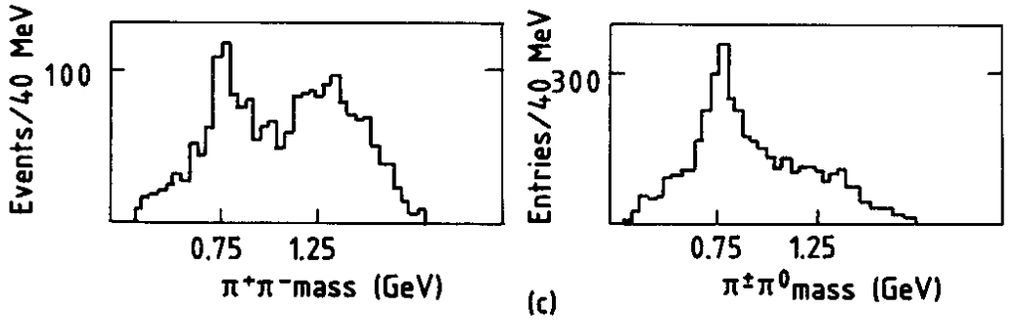
Events/40 MeV
100
0.75
1.25
π⁺π⁻mass (GeV)
Entries/40 MeV
300
0.75
1.25
π±π⁰mass (GeV)

(c)

Fig. 16

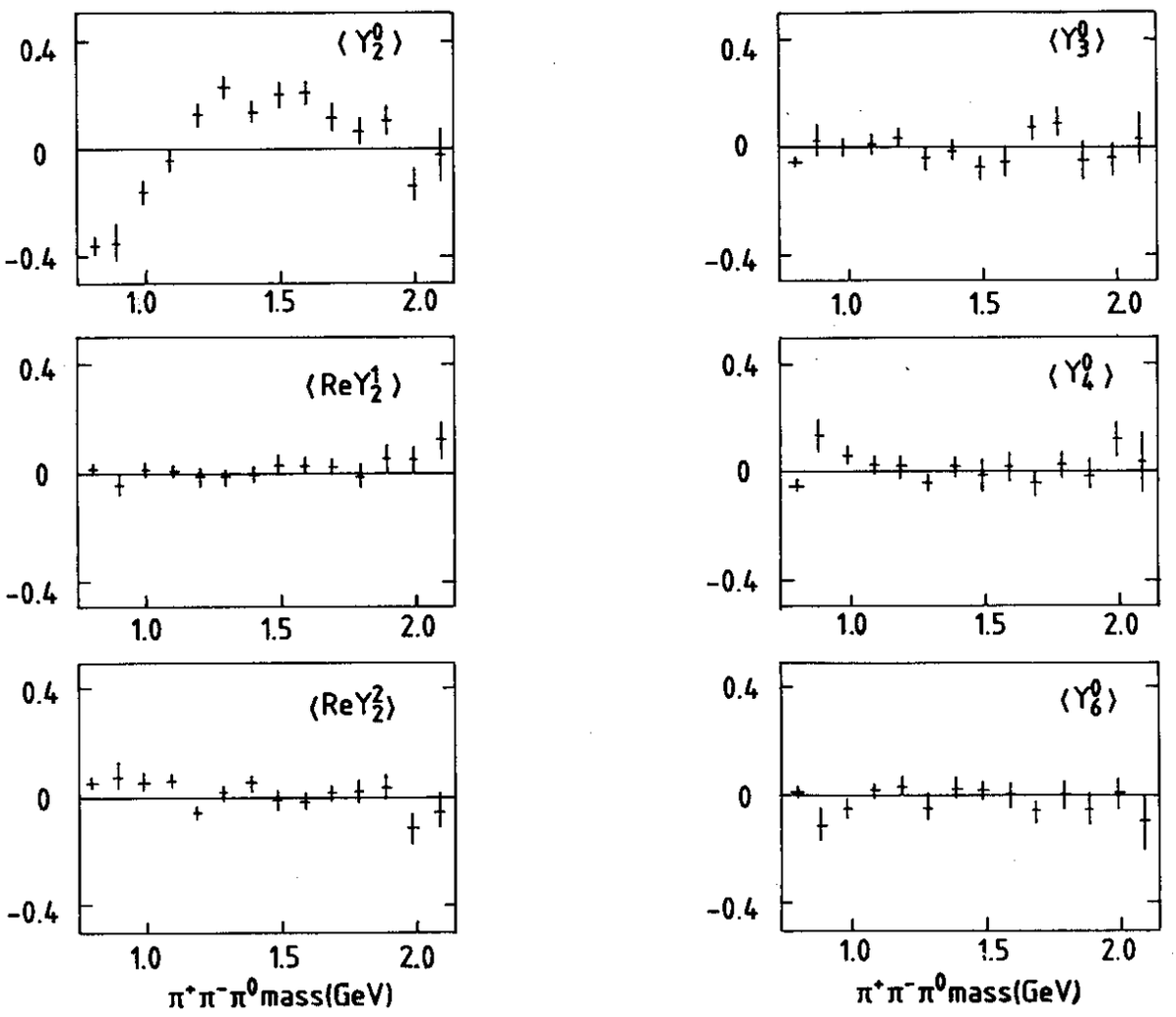

Fig. 17

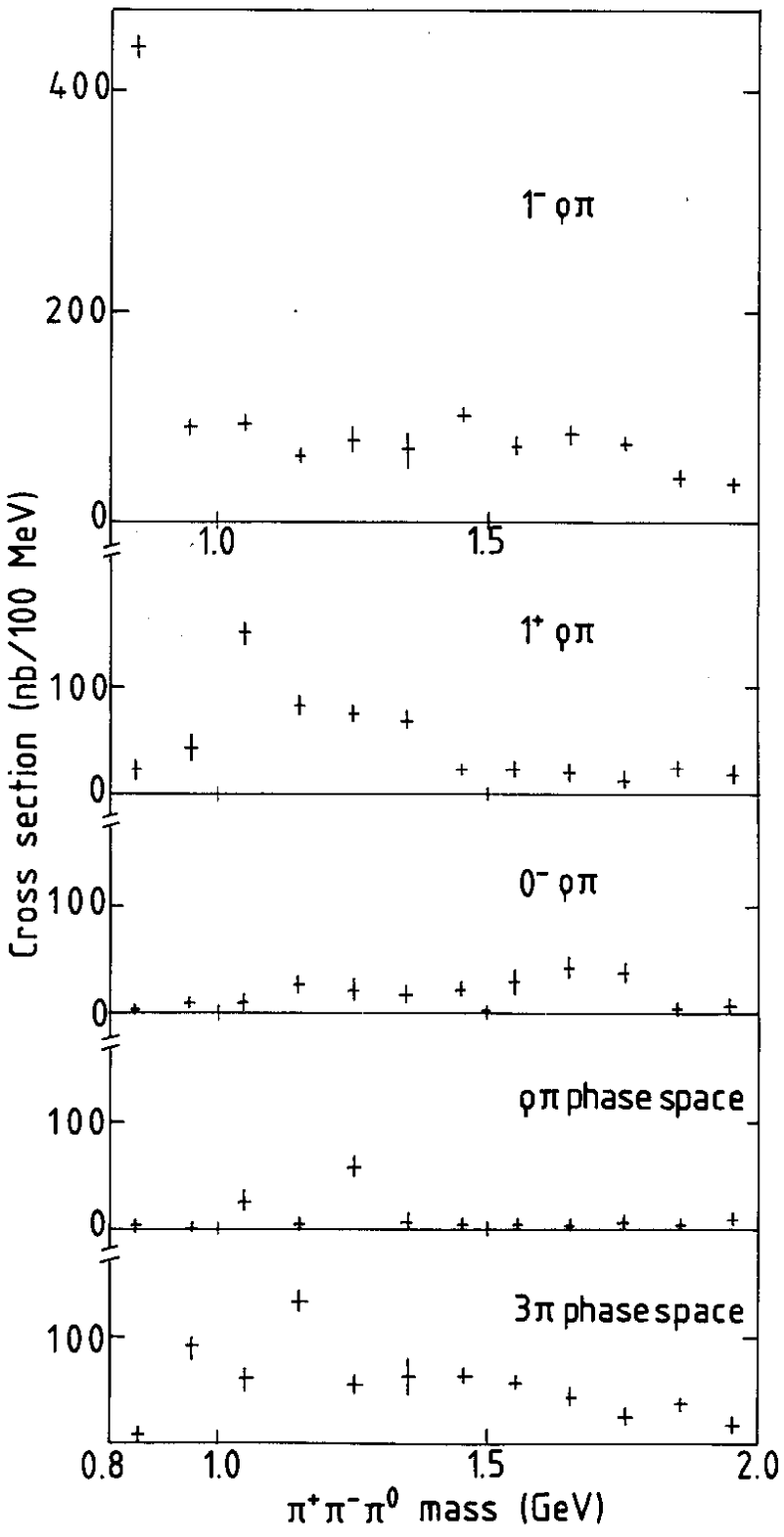
400
200
0
1⁻ ρπ
1.0
1.5
1⁺ ρπ
100
0
0⁻ ρπ
ρπ phase space
3π phase space
0.8
2.0
Cross section (nb/100 MeV)
π⁺π⁻π⁰ mass (GeV)

Fig. 18

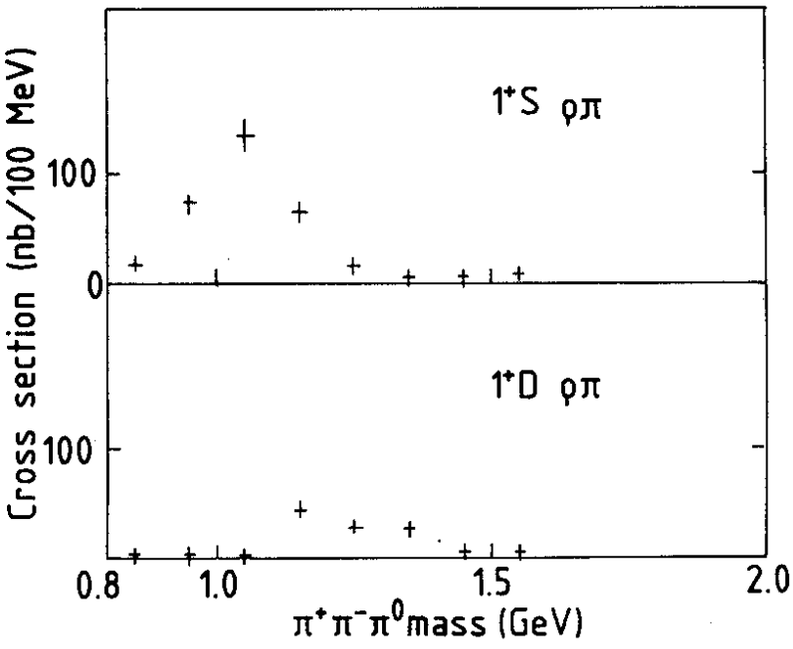
1⁺S ρπ
1⁺D ρπ
100
0
100
Cross section (nb/100 MeV)
0.8
1.0
1.5
2.0
π⁺π⁻π⁰mass (GeV)

Fig. 19

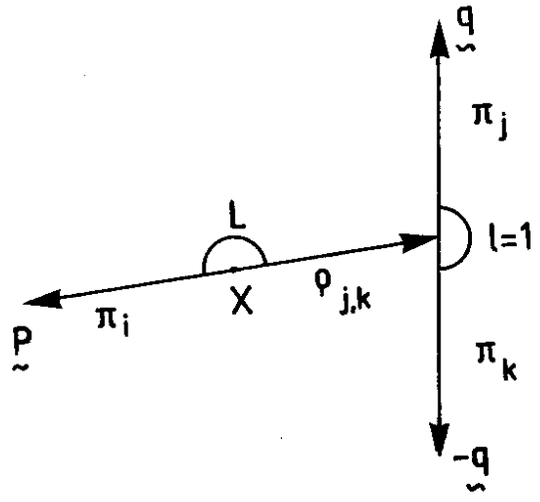
q
π_j
L
l=1
X
ρ_j,k
π_i
P
π_k
-q

Fig. 20